Journal of Sound and Vibration 432 (2018) 621–632

Contents lists available at ScienceDirect

Journal of Sound and Vibration

journal homepage: www.elsevier.com/locate/jsvi

The effect on vowel directivity patterns of higher order propagation modes

Rémi Blandin [a,*], Annemie Van Hirtum [b], Xavier Pelorson [b], Rafael Laboissière [c]

[a] GIPSA-Lab, UMR CNRS 5216, Grenoble Alpes University, 11 rue des Mathématiques (BP46), 38402 Grenoble, France
[b] LEGI, UMR CNRS 5519, Grenoble Alpes University, 38058 Grenoble, France
[c] LPNC, UMR CNRS 5105, Grenoble Alpes University, (BP47), 38040 Grenoble, France

ARTICLE INFO

Article history:
Received 4 October 2017
Revised 15 June 2018
Accepted 22 June 2018
Available online XXX
Handling Editor: R. E. Musafir

Keywords:
Speech
Vocal tract
Waveguide
Higher order mode
Vowel
Directivity

ABSTRACT

Measurements of speech directivity patterns show that it differs according to the phoneme pronounced. In the case of the vowels, these differences can be attributed to variations of the vocal tract shape. The multimodal method, which takes into account higher order propagation modes, is used to simulate directivity patterns (2 kHz–15 kHz) for simplified vocal tract geometries of the vowels [a], [e], [i], [o] and [u]. The directivity patterns of a simplified and a realistic replica of the vowel [a] are measured experimentally. The comparison of the experimental data with the simulations shows a good agreement (average difference of 1.7 dB). It is observed that the amplitude, orientation and number of lobes can change significantly for some small frequency intervals, of the order of 100 Hz; these are shown to be caused by higher order modes. These changes can occur as low as 3 kHz if a wide cavity is present near the mouth exit. A small mouth exit limits the effect to specific frequency intervals, and a narrow channel limits the transmission of the higher order mode effect to the mouth exit. The comparison of the directivity measured on a realistic replica corresponding to the vowel [a] with simulations performed on two simplified geometries shows that a fully asymmetric shape (for which the centers of the cross-sectional contours are not aligned) is qualitatively more realistic than a partially asymmetric shape (when the centers of the cross-sectional contours lie along the same axis).

1. Introduction

The speech directivity consists in the variation of the amplitude of the sound radiated by a speaker with the direction. It is important for various applications including microphone placement [1], telecommunication [2], vocal performance practice [3–5], architectural acoustics [6], auralization and 3D sound synthesis [7–9]. Directivity patterns have been measured experimentally on human subjects [1,3–5,10] as well as modelled physically [2,11,12]. It was observed that they are almost omnidirectional at low frequencies (of the order of 100 Hz) and that they become more complex and directional at higher frequencies (starting at 500 Hz).

Whereas speech directivity has been mostly considered for words and sentences, some studies highlighted differences between the directivity patterns of different phones. Marshall and Meyer [4] observed a difference between the directivity patterns of vowels [a], [o] and [e]. Halkosaari [2] also reported differences between vowels and related it to the difference of mouth aperture size. Likewise, for the fricatives, Monson et al. [5] observed differences between [s], [ʃ], [f] and [θ]. Katz et al. [10]

* Corresponding author.
E-mail address: remi.blandin@gmail.com (R. Blandin).

https://doi.org/10.1016/j.jsv.2018.06.053
0022-460X/

showed differences for both vowels and fricatives in a study specifically dedicated to the radiation patterns of the phones. On the other hand, higher order propagation modes (HOM) are present inside the vocal tract [13,14] above 3 kHz, and it is known that they can influence significantly the radiation of ducts [15–18]. It has been shown on simplified vocal tract geometries corresponding to the vowel [a] that HOM can influence significantly the directivity [19]. Thus, HOM could play an significant role for high-frequency speech directivity (above 3 kHz).

With the progress of technologies and applications, the increase of quality requirements necessitates a better knowledge of the physics underlying high-frequency speech radiation. Indeed, the simple physical models of speech directivity [2,11,12] account only for the external reflections, the diffraction by the head and the diffraction of the plane wave at the mouth exit. So the only parameter specific to a particular phone is the mouth exit cross-sectional area. The effect of the lips shape, the mouth exit cross-sectional shape and the three-dimensional (3D) aspect of the internal acoustic field in high-frequency are not considered. Thus, they cannot be used to predict accurately the directivity pattern of a specific phone for frequencies up to 15 kHz. On the other hand, directivity measurements are usually performed with a minimal frequency resolution of third-octave bands and with a minimal angular resolution of the order of 10°. This may mask phenomena related to the presence of HOM which occur within smaller frequency intervals and angular regions as reported in Ref. [19].

The objective of this work is to study the influence of the HOM, without other directivity mechanisms, on the directivity patterns for the vowels [a], [e], [i], [o] and [u]. Simulated directivity patterns of simplified vowel geometries are compared to each other and to measurements performed on mechanical replicas. The aim is also to provide a method which allows one to account for HOM while relying on simplified geometries and reasonable computational complexity in order to make systematic studies possible. For this purpose, the multimodal method (MM) [20–23] is used to predict the particle velocity distribution at the mouth exit at a relatively low computational cost compared to finite element or finite difference methods [14]. The radiated acoustic pressure is then calculated with the Rayleigh-Sommerfeld integral accounting for this distribution. In order to observe the directivity patterns accurately, the frequency range and the angular resolution of the measurements and the simulations have been set to 2–15 kHz and 2° respectively. Simplified geometries are designed from area functions provided by Story [24]. The design is made so that as much HOM as possible are elicited. Elliptical cross-sections are used as a simple way to take into account the width and height of the lip opening provided by Fromkin [25]. Eccentric junctions (*i.e.* the centers of consecutive contours are not aligned) are used in order to elicit as much as possible the HOM as it prevents cancelation of HOM due to symmetry [14,19].

The reliability of the simulation method is first assessed comparing simulations and experiments on a vowel [a] simplified geometry. Then, MM is applied to five simplified vowel geometries corresponding to [a], [e], [i], [o] and [u], in order to study the effect of HOM on these different vowels. Finally, the effectiveness to reproduce the effect of the HOM of the simplified geometries is evaluated for the vowel [a] by comparing the simulated directivity patterns with that measured on a realistic replica designed from magnetic resonance images (MRI) [26]. The vowel [a] is used since it has the largest mouth exit cross-section area and hence the effect of HOM is expected to be significant [19].

The paper is structured as follows: first the geometries, the experimental setup, the simulation method and the data analysis are detailed in section 2. Then, the results obtained from the comparison between simulation and experiment, the simulation for the vowels [a], [e], [i], [o] and [u] and the comparison between the simplified geometries and the realistic one are presented in section 3. Finally, the agreement between the simulations and the experiments, the relationship between the observed directivity patterns and the shape of the geometries, and the similarities between the simplified geometries and the realistic one are discussed in section 4.

2. Methods

This section presents the methods used to acquire and analyse the experimental and simulated data presented in section 3. These data consist of the acoustic pressure radiated by vocal tract geometries at different angular positions (spatial sampling each 2°) between 2 kHz and 15 kHz (frequency sampling every 10 Hz). The design of the geometrical approximations and the experimental setup are detailed in sections 2.1 and 2.2 respectively. An improvement of the implementation of the MM with respect to the previous works [14,19] is presented in section 2.3. Finally, the data analysis method is detailed in section 2.4.

2.1. Geometries

In order to perform simulations and experiments, different geometries approximating the shape of the vocal tract for the vowels [a], [e], [i], [o] and [u] are used. They are designed from area functions provided by Story [24] and from a 3D geometry extracted from MRI provided by Aalto et al. [26].

A 3D view of the simplified geometries is provided in Fig. 1. They are designed in order to exhibit HOM with cut-on frequencies of the same order of magnitude as for realistic geometries. They are constituted of 44 constant length tubes whose cross-sectional area is provided by area functions from Story [24]. Since the mouth exit cross-sectional shape is prominent for radiation problems, it is schematized as an ellips with a width to height ratio of the same order of magnitude as real subjects. In this purpose, the average ratios of 4 subjects presented in Fig. 5 of Fromkin [25] are used. Since no information about the internal cross-sectional shape is provided by Story [24], this ratio is kept constant for all the tubes for a given vowel. For each tube, elliptical shapes having the same area as the one provided by Story [24] are generated with the ratio averaged on Fromkin data [25]. The width and height of the mouth opening, the corresponding ratio and the length of the tubes are presented in

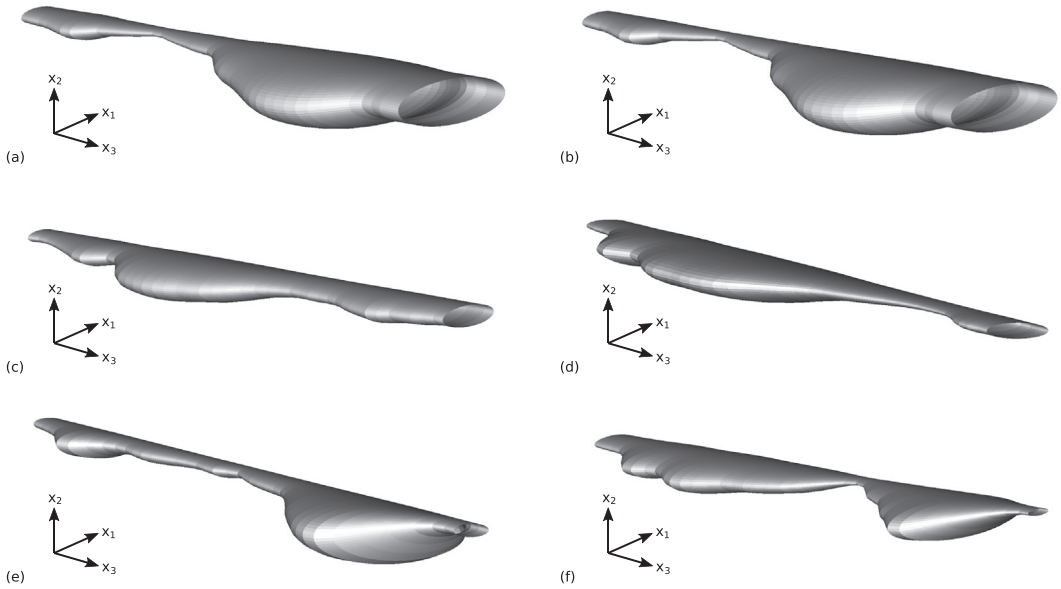

Fig. 1. Vocal tract geometries used for the simulations. The left side corresponds to the vocal fold location and the right side to the mouth exit. (a) Vowel [a] symmetric with respect to the plane (x_2, x_3) (symmetric [a]); (b) vowel [a] (fully asymmetric [a]); (c) vowel [e]; (d) vowel [i]; (e) vowel [o]; (f) vowel [u].

Table 1
Features of the elliptical cross-sectional shape of vocal tract geometries designed as concatenations of 44 tubes from area functions corresponding to the vowels [a], [e], [i], [o] and [u]: width (along x_1), height (along x_2) at the mouth aperture, ratio of width over height provided by Ref. [25] and length along x_3 of the tubes.

Vowel	[a]	[e]	[i]	[o]	[u]
Width along x_1 at mouth exit (mm)	44.2	20.2	25	14.64	9.32
Height along x_2 at mouth exit (mm)	13.6	6.00	4.62	4.08	2.18
Ratio of width over height	3.25	3.35	5.43	3.58	4.27
Length along x_3 of the tubes (mm)	3.85	3.84	3.81	4.09	4.38

Table 1. The length of the tubes is kept constant for a given vowel.

In order to elicit as much HOM as possible, the centers of the cross-sections are shifted along both axis x_2 and x_1. The contours are aligned so that their highest point along x_2 is contained in a common plane (x_1, x_3). Thus, the coordinate x_2^n of the center of the tube n are shifted so that $x_2^n = h_{44} - h_n$ with $n \in [1, 43]$, h_n being the height of the elliptical shape. The center of the cross-section corresponding to the mouth is placed at the origin of the landmark: $x_1^{44} = x_2^{44} = 0$. Along x_1, 25% of eccentricity is introduced. The value 25% has been set arbitrarily as a rough adjustment so that the directivity patterns of the fully asymmetric [a] are qualitatively similar (above 3 kHz) to the experimental ones obtained with the realistic replica of the vowel [a]. A too high eccentricity would exaggerate the effect of HOM and a too small eccentricity would underestimate their effect [19]. The coordinate x_1^n of the center of the tube n is shifted so that $x_1^n = -0.25 \times (w_{44} - w_n)$ with $n \in [1, 43]$, w_n being the width of the elliptical shape. As a reference, an additional geometry is created for the vowel [a] with all the cross-sections sharing a common line on the top in the plane (x_2, x_3) and all cross-sections centred in the plane (x_1, x_3) (see Fig. 1a). This geometry is referred to as symmetric [a] hereafter. For all the geometries designed from area functions, the length of the tubes provided in Ref. [24], is modified (see Table 1) so that the length of the line which connects the centers of all the tubes, the center-line, is the same as the original length provided in Ref. [24] *i.e* 170.9 mm, 169.8 mm, 169.0 mm, 183.3 mm and 195.9 mm for [a], [e], [i], [o] and [u] respectively. This is done to compensate a shift down of the formant frequencies (down to 2%) which occurs without adjustment. The mouth exit of these simplified geometries is considered to be located at the junction between the upper and the lower lips, *i.e.* the corner of the lips.

In order to perform measurements for the validation of the simulation method a mechanical replica of symmetric vowel [a] geometry (see Fig. 1a) has been 3D printed (see Fig. 2a). This has been done with a 3D printer ProJet 3510 SD with accuracy 0.025 mm–0.05 mm per 25.4 mm. The thickness of the walls of the replicas is 5 mm. Likewise, in order to study a more realistic vocal tract shape which cannot be simulated with the implemented MM method (see section 2.3) due to the curvature of the vocal tract shape and the lips, the 3D shape provided by Aalto et al. [26] for the vowel [a], has been 3D printed. This realistic vocal tract geometry is the only one throughout based on a single subject. To do so, the trachea and the face have been removed and a 5 mm thickness has been added as well as fittings for a sound source and a rectangular flange allowing one to attach a Plexiglas baffle (see Fig. 2b).

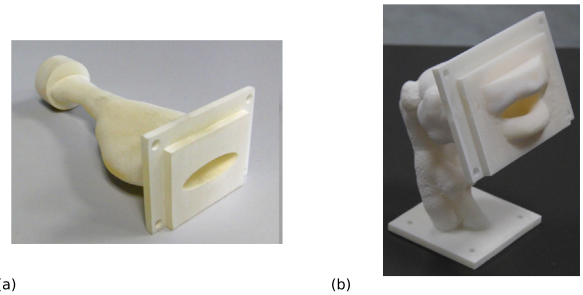

(a) (b)

Fig. 2. Mechanical replicas used to perform acoustic measurements. (a) Vowel [a] symmetric with respect to the plane (x_2, x_3) designed from an area function from Story [24] (symmetric [a]); (b) vowel [a] from MRI from Aalto [26] (realistic [a]).

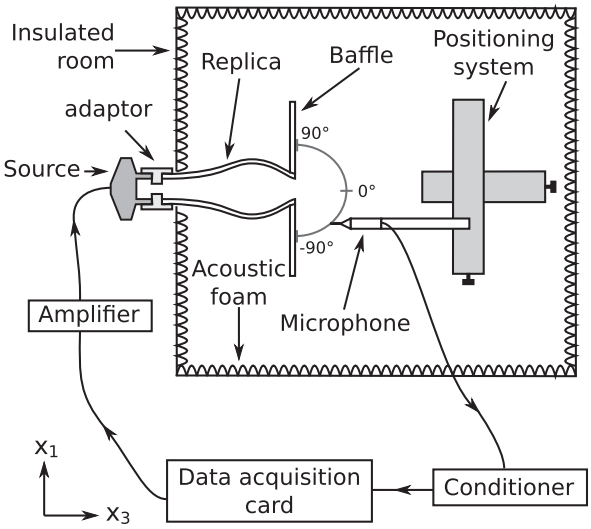

Fig. 3. Schematic overview of the experimental setup used to measure the directivity patterns of the vocal tract replicas. The replicas are mounted with the same orientation as in Fig. 1.

2.2. Experimental setup

An experimental setup is designed in order to measure the acoustic pressure at various locations outside the replicas. A schematic diagram of it is presented in Fig. 3.

Sounds are generated at the entrance (vocal fold side) of the replica with a compression chamber (Eminence PSD:2002S-8) which is connected to the replicas by an adaptor which features a 2 mm diameter centred communication hole from which the sound radiates inside the replicas. Linear sweeps going from 2 kHz to 15 kHz in 30 s are used.

The acoustic pressure is measured with a B&K 4182 probe microphone equipped with a 1 mm in diameter and 25 mm long probe, and connected to a B&K 4192 microphone conditioner. This microphone is moved by a positioning system (OWIS PS35) with an accuracy of ± 0.1 mm, however this accuracy can be reduced by the initial positioning which is less accurate (± 1 mm) and can induce a systematic error. All the measurements are performed on 91 points equally distributed (each 2°) in the plane (x_1, x_3) on a half circle of radius 40 mm centred on the exit of the replicas. This radius is imposed by the limitation of the experimental setup. The replicas are mounted following the orientation (x_1, x_2, x_3) shown in Fig. 1.

The signal V_m recorded by the microphone is transmitted to a data acquisition card (NI PCI-MIO 16 XE) and sampled at a frequency of 44.15 kHz. The same card is used to generate the excitation signal transmitted to an amplifier (Onkyo a-807) and then to the compression chamber. The whole process is controlled by a Labview (NI) program.

The open end of the replicas, the microphone and the positioning system are placed inside an insulated room ($1.92 \times 1.94 \times 1.99$ m, Vol = 7.45 m^3, [27]). Even though this room cannot be considered as perfectly anechoic, its acoustic characteristics in the frequency range of interest (2 kHz–15 kHz) are sufficient to consider that the influence of external noise can be neglected and that the free field assumption can be used. Indeed, the direct field has an higher amplitude than the reverberated field up to 0.94 m from the exit of the replica and the attenuation of the external noise is greater than 25 dB SPL [27].

Acoustic foam is placed on the table supporting the positioning system and on the positioning system itself in order to damp the first reflections. The acoustic source is placed outside of the insulated room to avoid interference between the sound directly

radiated by the compression chamber and the sound radiated by the replica. A rigid Plexiglas rectangular baffle (365 × 360 mm) is attached to the exit of the replica (mouth side) to approximate the infinite baffle assumption implemented in the simulation method and to act as a very rough approximation of the face. The temperature inside the insulated room is measured with a precision of ±0.1°C.

2.3. Simulations

The MM presented in Refs. [14,19,28] is used to simulate the acoustic pressure radiated by the different geometries. This implementation is limited to discrete straight waveguides with arbitrary cross-sections set in an infinite baffle.

In order to reduce the computational cost and to improve the accuracy of the simulations, the implementation is modified so that the resolution of the grid is adapted to the size of the different cross-sections. For each cross-section, the minimal distance $r_{\min}$ between the center of the cross-section and the edge is computed. The spacing Δx between the points of the grid at a given cross-section is defined as

$$\Delta x = \frac{r_{\min}}{N_{\min}},$$

$N_{\min}$ being the number of points along the segment linking the center of the contour and the closest edge. $N_{\min}$ is kept constant for all the cross-sections. Indeed, this allows one to compute more accurately the propagation modes in the small cross-sections without requiring a great number of points in the large cross-sections. Thus, for a given accuracy it requires less computation than for a grid with constant spacing. On the other hand, a constant resolution induced an in-homogeneity of the accuracy of the computation of the propagation modes which was detrimental for the accuracy of the computation. Indeed, the propagation modes were computed with a better accuracy in the large cross-sections than in the small cross-sections. However, the lower accuracy obtained on the small cross-sections affected the whole computation.

The convergence of this new implementation has been assessed performing simulations with different $N_{\min}$. The simulations presented here have been performed with $N_{\min} = 40$ *i.e.* $0.03 \leq \Delta x \leq 0.24$ mm. Inside each tube of the geometries all the HOM having a cut-on frequency comprised between 0 kHz and 50 kHz are used. The convergence has also been assessed with the number of HOM performing simulations with different upper frequency boundary for the computation of the HOM. The source (vocal fold side) is modelled by a circular surface of 2 mm in diameter located at the center of the first cross-section on which the particle velocity is set equal to 1. A Neumann boundary condition is used on the contour of the cross-sections in order to model hard walls. At the exit (mouth side) an infinite baffle condition is considered. The radiated pressure is simulated between 2 kHz and 15 kHz every 10 Hz.

Previously [14], the MM simulation method was validated to simulate the acoustic pressure field inside vocal tract geometries including the symmetric [a]. In addition, qualitative good agreement of the directivity pattern was obtained for concentric (2 tube and 44 tubes) and eccentric (2 tubes and 44 tubes) circular approximations of vowel [a] [19]. However, it was seen that a higher spatial measurement accuracy was needed in order to confirm this quantitatively. A quantitative validation of the directivity patterns is therefore assessed in sections 3.1 and 4.1.

In the case of the symmetric [a] (see Figs. 1a and 2a), the acoustic pressure is simulated at the same locations as the measurements: on 91 points equally distributed in the plane (x_1, x_3) on a half circle of radius 40 mm centred on the exit of the replicas. For the other geometries, the radius is increased to 600 mm, which is closer to the distance corresponding to a conversation [29].

For the sake of brevity, the directivity maps simulated at 40 mm of the exit of the fully asymmetric geometries are not presented here. Indeed, no significant difference between the directivity simulated at 40 mm and 600 mm is expected since both distances are in the far field from Fresnel diffraction point of view. The Fresnel parameter S allows one to make the distinction between near field and far field [30]. It is defined as $S = \frac{r\lambda}{(w_{44}/2)^2}$, r being the distance from the center of the exit, λ the wavelength and w_{44} the width of the last section. The far field is considered to start at $S \geq 1$. In the case of 15 kHz at 20°C and $r = 40$ mm, $S = 1.9$ for the widest exit. So, the far field assumption holds. However, this is true for a uniform pressure field at the exit and HOM create more complex diffraction patterns. Thus, the average of the absolute difference between the directivity maps simulated at 40 mm and 600 mm has been computed in order to quantify the variations with the distance. This is less than 2 dB, which confirms that there are no significant differences between measurements or simulations at these two distances.

2.4. Data analysis

For the experimental data, the relative amplitude of the acoustic pressure is estimated from the sweep signal using Fourier transform. The signal is sliced in windows of 2048 samples (46.4 ms) overlapping each other by 50%. A Hann window is applied in order to limit the artifacts due to the small duration of the window [31]. Then, the maximum spectral amplitude is sought inside an interval of 100 Hz centred on the middle frequency of the sweep signal inside each window. This allows one to remove the harmonics generated by the nonlinearities of the sound source. The influence of the nonlinearities and the repeatability of the measurement have been assessed (sections 3.3.2 and 3.3.3 of [28]).

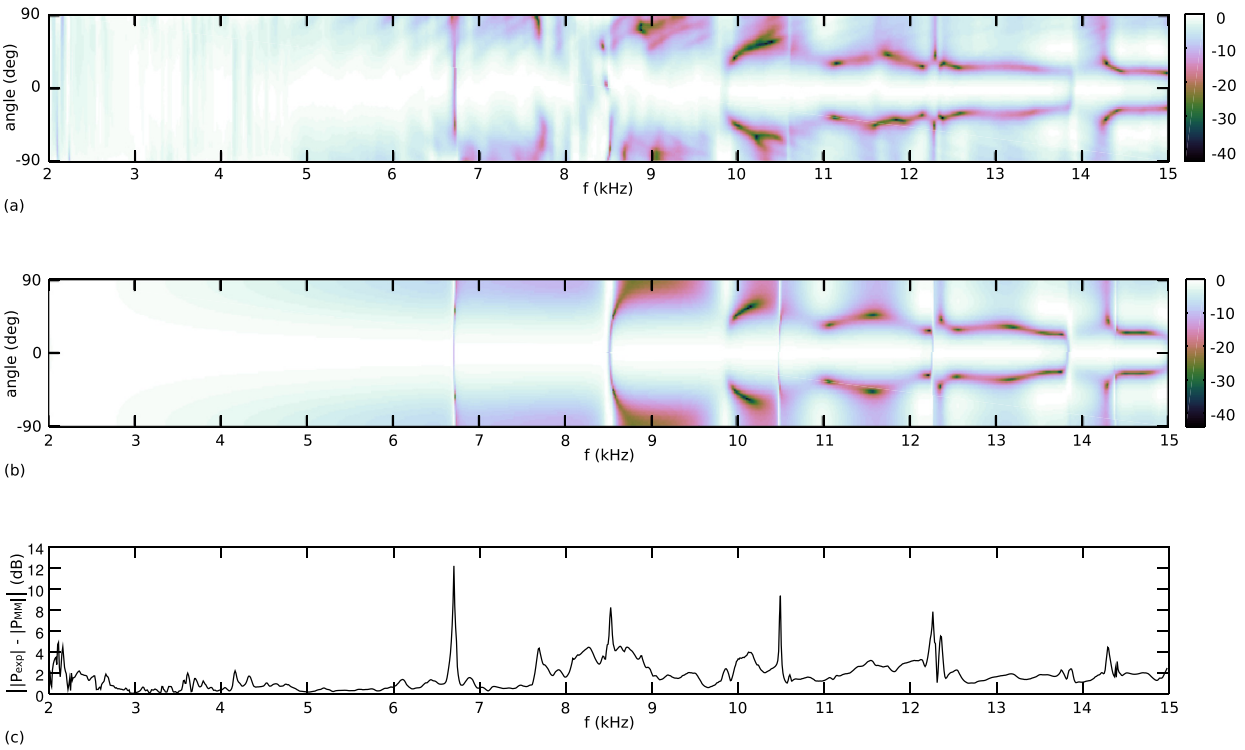

Fig. 4. Normalized amplitude of acoustic pressure P as a function of frequency and angular position measured $|P_{exp}|$ and simulated $|P_{MM}|$ in the horizontal plane (x_1, x_3) at 40 mm from the exit of a simplified vocal tract symmetrical [a] geometry shown in Fig. 1a. The difference between the measured and simulated directivity pattern averaged on the angular position $|P_{exp}| - |P_{MM}|$ is presented as a function of frequency. (a) Experiment $|P_{exp}|$; (b) MM simulation $|P_{MM}|$; (c) difference between the amplitude of the experiment and the simulation averaged over the angular position $|P_{exp}| - |P_{MM}|$.

In order to highlight the change of amplitude related to the angular position, the amplitude is normalized by the maximum of amplitude over the positions at each frequency. Directivity maps showing the variations of the directivity pattern with the frequency are thus obtained (see Figs. 4–6). In order to quantify the directivity at given frequencies, the difference between the maximum and the minimum of amplitude over the positions is computed. This quantity is referred to as maximal sound pressure level difference (MSPLD) hereafter.

3. Results

In this section the data obtained from the experiments and the simulations are presented in the form of directivity maps in Figs. 4–6. First, the experiment and the simulation for the symmetric [a] are compared in section 3.1 in order to assess the reliability of the simulations. Then the simulation method is applied to the fully asymmetric geometries of the vowels [a], [e], [i], [o] and [u] in section 3.2. Finally, the directivity of the realistic replica of the vowel [a] is presented in section 3.3. A discussion of these results is provided in section 4.

3.1. Comparison between simulation and experiment

Fig. 4 presents the directivity maps measured with the symmetric [a] replica (see Fig. 4a) and simulated with the same geometry (see Fig. 4b). The difference between both maps averaged over the angular positions for each frequency is presented in Fig. 4c.

In the experimental data (see Fig. 4a), the directivity pattern tends to be uniform with small variations visible as vertical streaks up to about 4.6 kHz. Above this frequency, a one lobe pattern which becomes more pronounced as the frequency increases is visible up to 9.7 kHz. After this frequency a three lobes pattern appears. Likewise, in the simulation data (see Fig. 4b), a one lobe pattern is visible from 2.8 kHz to 9.4 kHz, which becomes more pronounced as the frequency increases. Above 9.4 kHz it becomes a three lobes pattern. The directivity patterns are perfectly symmetric in the case of the simulation while they show small asymmetries in the case of the experiment.

Above 6.7 kHz, the directivity patterns, both measured and simulated, become more complex. Significant variations of the MSPLD, the number of lobes, the position and the size of the lobes occur within small frequency variations (order of 100 Hz). This is observed in particular at 6.69 kHz, 8.48 kHz, 10.60 kHz, 12.28 kHz and 13.92 kHz for the experiment and at 6.71 kHz, 8.48 kHz,

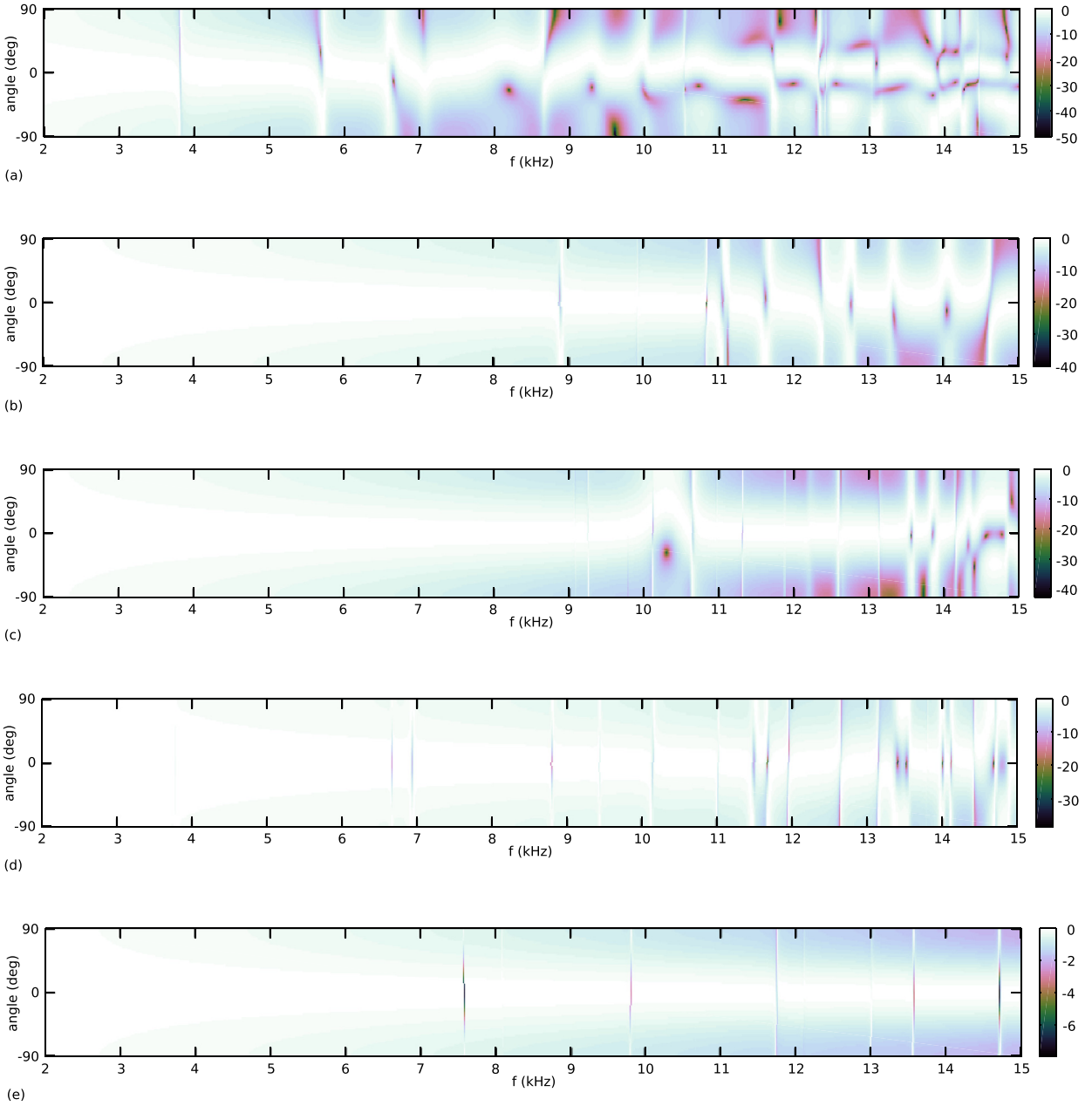

Fig. 5. Normalized amplitude of the acoustic pressure as a function of frequency and angular position simulated in the horizontal plane (x_1, x_3) at 600 mm from the exit of five simplified vocal tract geometries corresponding to [a], [e], [i], [o] and [u] shown in Fig. 1b, 1c, 1d, 1e and 1f. (a) Vowel [a]; (b) vowel [e]; (c) vowel [i]; (d) vowel [o]; (e) vowel [u].

10.49 kHz, 12.26 kHz, 13.80 kHz and 14.38 kHz for the simulation. One can also see transitions between almost omnidirectional patterns (MSPLD smaller than 4 dB) and very directional patterns (MSPLD greater than 40 dB).

The averaged difference between the experiment and the simulation (see Fig. 4c) is less than 5 dB, except for some peaks which appears at frequencies corresponding to significant change of the directivity pattern within a small frequency interval (at 6.7 kHz, 8.52 kHz, 10.49 kHz, 12.26 kHz and 12.35 kHz). The difference averaged on all the position and frequencies is of 1.7 dB. The averaged difference is globally higher between 7.5 kHz and 15 kHz. This can be related to the greater complexity of the directivity patterns and their variations as well as the more pronounced minima of amplitude in this interval.

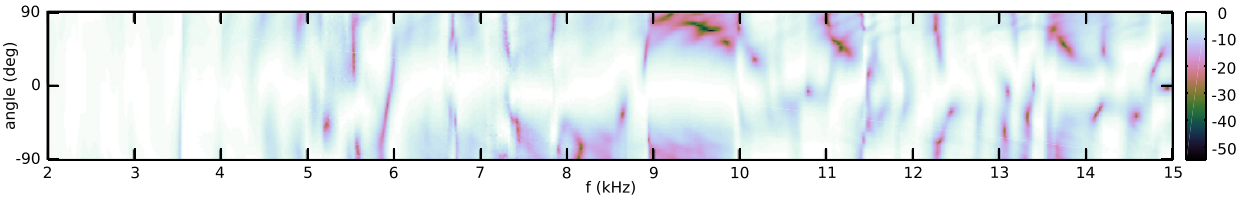

Fig. 6. Normalized amplitude of the acoustic pressure as a function of frequency angular position measured in the horizontal plane (x_1, x_3) at 40 mm from the exit of a vowel [a] vocal tract replica (see Fig. 2b) built from MRI [26].

3.2. Simulation of the directivity for five vowels

Fig. 5 presents the directivity maps simulated with the geometries corresponding to the vowels [a], [e], [i], [o] and [u], shown in Fig. 1b, 1c, 1d, 1e and 1f.

For all the geometries, there is a one lobe symmetric pattern (maximum between −10°and10°) which becomes more pronounced with the frequency, at least up to 6.5 kHz. The progressive augmentation of its amplitude (of the order of 0.1 dB per 100 Hz) as the frequency increases contrasts with significant variations of the directivity patterns localized in frequency intervals or in high-frequency. Indeed, significant change of the orientation (order of 50°), the number of lobes (up to 4), the amplitude of the lobes (up to 50 dB) of the directivity pattern occurs inside small frequency intervals (order of 100 Hz) and in high-frequency. In particular, transitions between almost omnidirectional patterns and more directional patterns occur within less than 100 Hz.

In the case of the vowel [a] (see Fig. 5a), the symmetric one lobe pattern is visible up to 6.5 kHz. It is interrupted by two significant variations which occur in intervals of about 500 Hz centred on 3.81 kHz and 5.68 kHz. Above 6.5 kHz the directivity patterns are asymmetric at all the frequencies. The variations of the directivity patterns increase in complexity with the frequency. There are significant changes within about 100 Hz at all the frequencies between 6.5 kHz and 15 kHz. Significant variations of the orientation of the lobes are observed, as an example, there is a variation of 68° between 6.54 kHz and 6.65 kHz. Likewise, significant variations of the orientation of the minima occurs, as an example, there is a variation of 88° between 8.63 kHz and 8.8 kHz. The number of lobes alternate between 1, 2, 3 and 4. There are transitions between quasi omnidirectional patterns (MSPLD down to 0.96 dB) and very directional patterns (MSPLD greater than 28 dB) within less than 70 Hz at 5.74 kHz and 6.58 kHz. The MSPLD reaches up to 50 dB at 14.25 kHz.

In the case of the vowel [e] (see Fig. 5b), the symmetric one lobe pattern can be seen up to 13.2 kHz, after which the patterns becomes fully asymmetric and more complex variations occur at all the frequencies. However, this pattern is interrupted by significant variations within frequency intervals up to 300 Hz wide centred on 8.89 kHz, 11.1 kHz, 11.62 kHz, 12.4 kHz and 12.77 kHz. Inside these intervals the directivity patterns are asymmetric. Significant changes within very small frequency intervals (order of 50 Hz) are also observed at 9.92 kHz and 10.84 kHz. Transitions between quasi-omnidirectional (MSPLD down to 0.85 dB) and directional (MSPLD greater than 15 dB) patterns within less than 70 Hz are observed at 8.9 kHz, 11.68 kHz, 12.4 kHz, 12.7 kHz and 12.81 kHz. A two lobes pattern appears occasionally inside intervals up to 200 Hz wide centred on 11.7 kHz, 12.4 kHz, 12.7 kHz 12.8 kHz, 13.3 kHz, 14 kHz, 14.1 kHz and 14.6 kHz.

In the directivity map of the vowel [i] (see Fig. 5c) the symmetric one lobe pattern can be seen up to 9.5 kHz and between 11 kHz and 13.4 kHz. Outside of this frequency region the patterns are asymmetric and the variations are more complex at all the frequencies. Between 9.6 kHz and 10.6 kHz one can observe the displacement of a maximum from 4° to 44° and back to −2° and the apparition of a two lobes pattern. Significant changes occur inside small intervals (up to 200 Hz) centred on 10.65 kHz, 12.2 kHz, 12.6 kHz and 13.14 kHz. Significant variations occur within very small frequency intervals (order of 50 Hz) centred on 9.08 kHz, 9.25 kHz, 9.79 kHz, 11.31 kHz and 11.87 kHz. Transitions between almost omnidirectional patterns (MSPLD down to 2.5 dB) and directional patterns (superior to 17 dB) within less than 100 Hz are observed at 12.6 kHz, 13.6 kHz, 13.9 kHz and 14.83 kHz. A two lobes pattern is present inside some of the small intervals containing significant variations, between 10.12 kHz and 10.48 kHz and above 13.4 kHz.

In the case of the vowel [o] (see Fig. 5d), the symmetric one lobe pattern can be seen up to 14.4 kHz after which asymmetric patterns with complex variations are visible. It is interrupted by significant variations between 11.4 kHz and 11.7 kHz, 13.1 kHz and 13.6 kHz, 13.9 kHz and 14.2 kHz, 14.4 kHz–15 kHz. Significant changes can also be seen within small frequency intervals (order of 100 Hz) centred on 6.94 kHz, 8.8 kHz, 9.43 kHz, 10.14 kHz, 11.49 kHz, 11.67 kHz, 11.95 kHz and 12.64 kHz, and within very small frequency intervals (order of 50 Hz) centred on 3.78 kHz, 6.66 kHz and 11 kHz. Transitions between quasi omnidirectional (MSPLD down to 0.15 dB) and more directional patterns (MSPLD greater than 8 dB) can be seen at 6.9 kHz, 11.45 kHz, 13,97 kHz and 14.89 kHz. A two lobes pattern appears inside each of the frequency intervals containing significant changes of directivity pattern, and above 14.4 kHz.

The directivity of the vowel [u] (see Fig. 5e) predominantly consists of a symmetric one lobe pattern. It is interrupted by significant variations within very small frequency intervals (order of 50 Hz) at 7.57 kHz, 8.09 kHz, 9.81 kHz, 11.74 kHz, 12.1 kHz, 13 kHz, 13.57 kHz and 14.71 kHz. Transitions between almost omnidirectional (MSPLD down to 0.2 dB) and more directional patterns (MSPLD greater than 3 dB) occur at 9.8 kHz, 13.56 kHz and 14.7 kHz. A two lobes pattern appears at 7.57 kHz, 9.81 kHz, 13.57 kHz and 14.71 kHz.

3.3. Directivity measurements for realistic vowel [a] replica

Fig. 6 shows the directivity map measured with the realistic vowel [a] vocal tract replica (see Fig. 2b). The directivity pattern exhibits one almost symmetric lobe up to 4 kHz (MSPLD inferior to 3 dB). It is interrupted by a significant change with a pronounced asymmetry within about 100 Hz around 3.5 kHz. Above 4 kHz strong asymmetries appear and the variations of the patterns become more and more complex as the frequency increases. Significant changes of the orientation (order of 50°), the number (up to 4), and the amplitude of the lobes occur within about 100 Hz. Particularly significant changes occur at 3.56 kHz, 5.96 kHz, 8.059 kHz, 11.49 kHz, 13.08 kHz and 13.39 kHz. Transitions between patterns with small directivity (MSPLD inferior to 10 dB) and patterns with prominent directivity (MSPLD of the order of 30 dB) occur within about 100 Hz, as an example at 5.6 kHz, 8.7 kHz, 10.2 kHz and 14.6 kHz.

4. Discussion

In this section, the results presented in section 3 are discussed. First, the validation of the simulation of the directivity patterns is discussed in section 4.1. Then, the directivity maps obtained for the vowels [a], [e], [i], [o] and [u] with fully asymmetric shapes are interpreted in terms of propagation of HOM and geometrical features in section 4.2. Finally, the measurements performed on the realistic [a] are compared to the simulations performed with the symmetric [a] and the fully asymmetric [a] in section 4.3.

4.1. Validation of the simulated directivity patterns

The directivity maps measured on the symmetric vowel [a] replica (see Fig. 4a) and simulated on the same geometry (see Fig. 4b) show similar patterns. The difference between both directivity maps is small: the averaged difference is less than 5 dB for most of the frequencies. The vertical streaks visible between 2 kHz and 4.6 kHz can be explained by the measurement noise which generates amplitude variations greater than the ones due to directivity, which is very weak in this frequency interval. This disrupts the normalization procedure which generates these patterns. Above 4.6 kHz the amplitude variations due to directivity becomes greater than the measurement noise and a one lobe pattern becomes visible. In both cases a symmetric one lobe pattern becoming more pronounced with the frequency can be seen up to 9 kHz. The small asymmetries present in the experimental data can be explained by small asymmetries of the experimental setup and measurement noise. The maxima and minima of the experiment and the simulation occur at frequencies and angular positions close to each other. The significant variations of the directivity pattern within small frequency interval occur at close frequencies. These small frequency difference (of the order of 100 Hz) are at the origin of the peaks of averaged difference. It may be explained by errors in the computation of the eigenfrequencies of the propagation modes due to the limit of the boundary condition model, numerical errors (see section 2.3) or inaccuracy of the temperature measurement (see section 2.2). It can be concluded from this comparison that the MM successfully predicts the directivity of the symmetric vowel [a] replica. This simulation method is thus considered as valid for the simulation of the directivity of other vocal tract geometries.

4.2. Comparison of the directivity of five vowels

In what follows, the concept of cut-on frequency is used in a local sense, *i.e.* at the scale of a section. It is used to indicate if HOM are damped in a section or not.

The five fully asymmetric vowel geometries generate very different directivity maps. However, all of them show, at least at low frequency (up to 6.5 kHz for [a]), a symmetric one lobe pattern which becomes more pronounced as the frequency increases. This can be attributed to the diffraction of the plane mode ([32], p226-227) which is present at all the frequencies. On the other hand, all the vowels generate significant variations of the directivity pattern within small frequency variations (of the order of 100 Hz). As shown previously [19], this is due to the influence of HOM, and it is similar to the directivity patterns theoretically predicted and observed with ducts when HOM are propagating [15–18]. These effects can appear on very wide frequency ranges (as for the vowel [a] at all the frequencies from 6.5 kHz) as well as on very narrow frequency intervals (as for the vowel [u], on intervals of the order of 50 Hz).

These phenomena are not observed yet in the measurements performed on human subjects [1,3–5,10]. Thus, it would be interesting to increase the frequency and angular resolution of these measurements. On the other hand, no strong asymmetry of the directivity patterns with respect to the mid-sagittal plane (x_2, x_3) are observed on human subjects as well. This is probably due to the averaging effect of octave and third octave bands analysis which may compensate asymmetries. Indeed, the significant variations, such as local minima, may be compensated by the remainder of the frequency band under analysis. Likewise, the asymmetries, such as local maxima on one side may be compensated in the same way. Thus, it would be interesting to analyse *in vivo* measurements with an increased frequency resolution and to perform others with an increased angular resolution in order to identify this phenomenon *in vivo*.

The vowel [a] geometry (see Fig. 1b) has a large cavity (62 mm in the widest part) directly connected to a wide mouth exit (44.2 mm, see Table 1). The HOM can propagate at low frequency (from 3.32 kHz) inside this cavity. Thus, they appear at lower frequency than in the geometries studied in Ref. [19] for which it starts at 6.5 kHz. This can be attributed to the elliptical shape

which induces lower cut-on frequencies [33] and to asymmetry of the geometry in both planes (x_1, x_3) and (x_2, x_3) which ensures that all the HOM are elicited. They affect directly the particle velocity distribution on the mouth exit and thus, the directivity patterns. As a consequence, their effect on the directivity can be seen from 3.7 kHz, and they affect the directivity at all the frequencies from 6.5 kHz onwards. On the other hand, the two intervals corresponding to the effect of HOM below 6.5 kHz are wider (about 500 Hz) than the first intervals in which HOM effect is visible for the other vowels (about 100 Hz). This can be explained by the fact that the vowel [a] has the widest mouth exit.

The vowels [e] and [i] have similar shapes (see Fig. 1c and d). A wide cavity (37.6 mm wide for [e] and 60 mm for [i]) is connected by a narrow channel (down to 18.4 mm wide for [e] and 15.6 mm for [i]) to the mouth exit. The channel becomes larger at the mouth exit forming a small cavity (26.3 mm for [e] and 25.7 mm for [i]). This cavity is divergent and then convergent in the case of the [e] whereas it is only divergent in the case of the [i].

The HOM can propagate from 5.46 kHz for [e] and 3.42 kHz for [i]. However, their effect on the directivity is visible only from 8.89 kHz for [e] and from 9.08 kHz for [i]. This is due to the fact that the narrow channel diminishes the influence of the HOM propagating inside the wide cavity on the particle velocity distribution at the mouth exit. Indeed, at the narrowest part of the channel, the HOM can propagate from 11 kHz for [e] and 13.3 kHz for [i]. As a consequence, the HOM propagating below these frequencies inside the wide cavity are exponentially damped. However, this damping is smaller for frequencies close to the cut-on frequency. On the other hand, when the frequency increases the distance on which no HOM propagation is possible reduces and is limited to the narrowest part of the channel. As a consequence, the HOM propagating inside the wide cavity can affect the directivity if their amplitude is particularly prominent and the frequency high enough. This can be seen as significant variations within very small frequency intervals (order of 50 Hz) at 9.92 kHz and 10.84 kHz for [e] and at 9.08 kHz, 9.25 kHz, 9.79 kHz, 11.31 kHz and 11.87 kHz for [i]. On the other hand, most of the effect of the HOM can be seen above 11 kHz for [e] and 13.4 kHz for [i]. This is due to the fact that the HOM propagating inside the wide cavity can influence more easily the directivity above the cut-on frequencies of the narrowest part of the channel.

In addition to the influence of the wide cavity, significant variations within wider frequency intervals (about 300 Hz for [e] and 1000 Hz for [i]) can be seen below the cut-on frequency of the narrowest part of the channel around 8.9 kHz and 10.1 kHz for [e] and [i] respectively. This is due to the propagation of HOM inside the small cavity at the mouth exit. Indeed, in this cavity HOM can propagate from 7.8 kHz for [e] and 8 kHz for [i]. This interval is wider for [i] (about 1000 Hz) than for [e]. Above the highest cut-on frequency of the channel, the effect of HOM tends to be localized in distinct intervals for [e] and to be spread over all the frequencies for [i]. This can be explained by the fact that the small cavity is divergent convergent for [e]. Indeed, this configuration has already been shown to reduce the effect of HOM on the directivity to narrower frequency intervals ([19], sections 4.1.5 and 4.2.10).

The vowels [o] and [u] have similar shapes (see Fig. 1e and f). A large cavity (62.6 mm wide for [o] and 55.9 mm wide for [u]) is directly connected to a narrow mouth exit (14.64 mm wide for [o] and 9.32 mm wide for [u], see Table 1). The HOM can propagate from low frequency (3.3 kHz for [o] and 3.7 kHz for [u]) inside the large cavity. However, their influence on the directivity is reduced by the small size of the mouth exit. Indeed, the HOM can propagate through the mouth exit from 14 kHz for [o] and 22 kHz for [u]. As for the vowels [e] and [i], the effect of HOM can be transmitted by evanescent HOM below the cut-on frequency of the mouth exit if the amplitude inside the wide cavity is high enough. However, in this case, the length of the constriction is smaller and the damping is less significant. As a consequence, the effect of HOM can be seen at lower frequencies, from 3.8 kHz for [o] and 7.6 kHz for [u]. The mouth exit of [u] being the smallest, the effect of HOM is concentrated in narrower intervals (order of 50 Hz). On the other hand, the damping diminishing as the frequency increases, one can see that the intervals corresponding to the effect of HOM become wider in the case of [o] as the frequency increases. This cannot be seen for [u] because the cut-on frequency of the mouth exit is much higher (22 kHz). Above 14.4 kHz the effect of HOM can be seen at all the frequencies for [o] because HOM can propagate through the mouth exit.

These simulations were performed with a hard wall assumption, however, vocal tract walls are not rigid. Simulations performed with non rigid walls [34,35] showed that, compared to rigid walls, the peak frequencies of the transfer function are shifted upward and their bandwidth is increased. However, this effect is shown to diminish as the frequency increase. Thus, it can be expected that with the introduction of non rigid boundary conditions, the effects of HOM on the directivity would be observed at different frequencies and in larger intervals. However, the differences are not expected to be significant at high frequency since the vocal tract walls behave more like hard walls.

4.3. Comparison of the directivity of a realistic replica of the vowel [a] and two geometrical simplifications

As stated in section 2.3, the average difference between the directivity map computed at 40 mm and the one computed at 600 mm (presented in Fig. 5a) is less than 2 dB. As a consequence, the comparison between the symmetric [a] measured and simulated at 40 mm (Fig. 3.1a and b) and the fully asymmetric [a] simulated at 600 mm (Fig. 5a) leads to the same conclusions as the comparison with the fully asymmetric [a] simulated at 40 mm.

The two geometrical approximations of the vowel [a] (see Fig. 1a and b) show very different directivity patterns. The directivity map of the symmetric [a] (see Fig. 4b) is rigorously symmetric whereas the directivity map of the asymmetric [a] (see Fig. 5a) is asymmetric at almost all the frequencies. The effect of HOM can be seen from lower frequency (3.7 kHz) for the asymmetric [a] than for the symmetric [a] (6.7 kHz). This is due to the fact that all the HOM which are symmetric with respect to the plane

(x_2, x_3) cannot be excited. Indeed, the contribution of the plane mode to excite the HOM compensates each other exactly in this configuration.

Similarly to the realistic replica, both the symmetric and the asymmetric [a] show significant variations of directivity pattern within small frequency variations (order of 100 Hz). However, the directivity of the realistic replica is qualitatively more similar to the one of the asymmetric [a]. Both are asymmetric at almost all the frequencies and the frequencies at which the effect of HOM starts to be visible are close (3.7 kHz for the asymmetric [a] and 3.5 kHz for the realistic [a]).

However, the directivity map of the realistic replica is different and more complex than the one of the asymmetric [a]. This can be explained by the more complex shape of the realistic replica and by the presence of the lips [36].

5. Conclusion

The simulations and the measurements have shown that HOM can affect significantly the directivity of simplified vowels. Thus, significant changes of the MSPLD, the orientation and the number of the lobes has been observed to occur within small frequency intervals (order of 100 Hz) for all the studied vowels in relation to HOM propagation. In order to observe this complex phenomenon, it is important to use small enough angular and frequency resolutions (2° and 10 Hz in this study).

The effect of HOM can be predominant in some frequency intervals for some vowels (all the frequencies from 6.5 kHz for the vowel [a]) and limited to very narrow frequency intervals for other vowels (a few intervals of the order of 50 Hz for the vowel [u]). The differences of vocal tract shape between the vowels induces significant differences in the directivity patterns. In addition, it is shown that one can qualitatively estimate the influence of the HOM from the shape of the vocal tract. Thus, a wide cavity will allow the HOM to propagate from relatively low frequency (down to 3.3 kHz). If this cavity is directly connected to a wide mouth exit, the effect will be present on a wide frequency range (all the frequencies from 6.5 kHz for [a]). On the contrary, if the mouth exit is small, the effect can be visible for low frequency (down to 3.8 kHz for [o]), but is limited to specific frequency intervals. Finally, if a wide cavity is connected to the mouth exit by a narrow channel, the effect of HOM propagating inside the wide cavity can be seen only in narrow intervals below the highest cut-on frequency of the channel and on wider frequency ranges above this frequency. The length of the channel will strongly limit the transmission of the effect at low frequency. As a consequence, the effect will be visible only at relatively high-frequency (from about 9 kHz for [e] and [i]).

The comparison with a measurement performed on a realistic replica showed that a fully asymmetric geometry has a directivity map qualitatively more similar to the one measured on a realistic replica than a partially asymmetric or a symmetric geometry. Thus, eccentricity in the transverse plane (defined by x_1 and x_2) is important to take into account.

These results highlight the importance of taking into account HOM for the simulation of directivity of vowels above the first HOM cut-on frequency (from 3 kHz). This also shows more broadly the importance of HOM on the directivity of waveguides when HOM can propagate. As a matter of fact, the simulation method and the prediction of the effect of HOM from the shape can be applied to any other waveguide geometry for different applications.

Acknowledgements

This research was supported by EU-FET Grant No. EUNISON 308874. The authors are grateful to Marc Arnela for the design of the 3D geometry of the realistic vocal tract replica.

Appendix A. Supplementary data

Supplementary data related to this article can be found at https://doi.org/10.1016/j.jsv.2018.06.053.

References

[1] H. Dunn, D. Farnsworth, Exploration of pressure field around the human head during speech, J. Acoust. Soc. Am. 10 (3) (1939) 184–199.
[2] T. Halkosaari, M. Vaalgamaa, M. Karjalainen, Directivity of artificial and human speech, J. Audio Eng. Soc. 53 (7/8) (2005) 620–631.
[3] D. Cabrera, P. Davis, A. Connolly, Long-term horizontal vocal directivity of opera singers: effects of singing projection and acoustic environment, J. Voice 25 (6) (2011) e291–e303.
[4] A. Marshall, J. Meyer, The directivity and auditory impressions of singers, Acta Acust united Ac 58 (3) (1985) 130–140.
[5] B. Monson, E. Hunter, B. Story, Horizontal directivity of low-and high-frequency energy in speech and singing, J. Acoust. Soc. Am. 132 (1) (2012) 433–441.
[6] F. McKendree, Directivity Indices of Human Talkers in English Speech, Inter-noise and NOISE-con Congress and Conference Proceedings, vol. 2, Institute of Noise Control Engineering, Cambridge, United States, 1986, pp. 911–916.
[7] L. Savioja, J. Huopaniemi, T. Lokki, R. Väänänen, Creating interactive virtual acoustic environments, J. Audio Eng. Soc. 47 (9) (1999) 675–705.
[8] J. Peng, T. Wang, S. Wu, Investigation on the effects of source directivity of Chinese speech intelligibility in real and virtual rooms, Appl. Acoust. 74 (8) (2013) 1037–1043.
[9] B. Postma, B. Katz, Creation and calibration method of acoustical models for historic virtual reality auralizations, Virtual Real. 19 (3–4) (2015) 161–180.
[10] B. Katz, C. d'Alessandro, Directivity measurements of the singing voice, in: 19th International Congress on Acoustics Madrid, Spain, 2007.
[11] J. Flanagan, Analog measurements of sound radiation from the mouth, J. Acoust. Soc. Am. 32 (12) (1960) 1613–1620.
[12] J. Huopaniemi, K. Kettunen, J. Rahkonen, Measurement and modeling techniques for directional sound radiation from the mouth, in: Applications of Signal Processing to Audio and Acoustics, 1999 IEEE Workshop on, IEEE, 1999, pp. 183–186.
[13] K. Motoki, N. Miki, N. Nagai, Measurement of sound-pressure distribution in replicas of the oral cavity, J. Acoust. Soc. Am. 92 (5) (1992) 2577–2585.
[14] R. Blandin, M. Arnela, R. Laboissière, X. Pelorson, O. Guasch, A. Van Hirtum, X. Laval, Effects of higher order propagation modes in vocal tract like geometries, J. Acoust. Soc. Am. 137 (2) (2015) 832–843.
[15] S. Savkar, Radiation of cylindrical duct acoustic modes with flow mismatch, J. Sound Vib. 42 (3) (1975) 363–386.
[16] R. Munt, The interaction of sound with a subsonic jet issuing from a semi-infinite cylindrical pipe, J. Fluid Mech. 83 (4) (1977) 609–640.

[17] A. Snakowska, H. Idczak, B. Bogusz, Modal analysis of the acoustic field radiated from an unflanged cylindrical duct–theory and measurement, Acta Acust united Ac 82 (2) (1996) 201–206.
[18] K. Kolber, L. Gorazd, A. Snakowska, J. Snakowski, The effect of cylindrical waveguide outlet features on the directivity pattern, in: Euronoise, 2015(Maastricht, The Netherlands).
[19] R. Blandin, A. Van Hirtum, X. Pelorson, R. Laboissière, Influence of higher order acoustical propagation modes on variable section waveguide directivity: application to vowel [], Acta Acust united Ac 102 (5) (2016) 918–929.
[20] A. Roure, Propagation guidée. etude des discontinuités (Guided propagation. Study of discontinuities), Ph.D. thesis, Université d'Aix-Marseille, 1976.
[21] J. Kergomard, A. Garcia, G. Tagui, J. Dalmont, Analysis of higher order mode effects in an expansion chamber using modal theory and equivalent electrical circuits, J. Sound Vib. 129 (3) (1989) 457–475.
[22] V. Pagneux, N. Amir, J. Kergomard, A study of wave propagation in varying cross-section waveguides by modal decomposition. Part I. Theory and validation, J. Acoust. Soc. Am. 100 (4) (1996) 2034–2048.
[23] J. Kemp, Theoretical and Experimental Study of Wave Propagation in Brass Musical Instruments, Ph.D. thesis, University of Edinburgh, 2002.
[24] B. Story, Comparison of magnetic resonance imaging-based vocal tract area functions obtained from the same speaker in 1994 and 2002, J. Acoust. Soc. Am. 123 (1) (2008) 327–335.
[25] V. Fromkin, Lip positions in American English vowels, Lang. Speech 7 (4) (1964) 215–225.
[26] D. Aalto, O. Aaltonen, R. Happonen, P. Jääsaari, A. Kivelä, J. Kuortti, J. Luukinen, J. Malinen, T. Murtola, R. Parkkola, et al., Large scale data acquisition of simultaneous MRI and speech, Appl. Acoust. 83 (2014) 64–75.
[27] A. Van Hirtum, Y. Fujiso, Insulation room for aero-acoustic experiments at moderate Reynolds and low Mach numbers, Appl. Acoust. 73 (1) (2012) 72–77.
[28] R. Blandin, Theoretical and Experimental Study of Vocal Tract Acoustics, Ph.D. thesis, Grenoble Alpes University, 2016.
[29] J.C. Baxter, Interpersonal spacing in natural settings, Sociometry (1970) 444–456.
[30] G.S. Kino, Acoustic Waves: Devices, Imaging and Analog Signal Processing, Prentice Hall, 2000.
[31] F. Harris, On the use of windows for harmonic analysis with the discrete Fourier transform, Proc. IEEE 66 (1) (1978) 51–83.
[32] A. Pierce, et al., Acoustics: an Introduction to its Physical Principles and Applications, vol. 20, McGraw-Hill New York, 1981.
[33] M.V. Lowson, S. Baskaran, Propagation of sound in elliptic ducts, J. Sound Vib. 38 (2) (1975) 185–194.
[34] K. Motoki, Three-dimensional rectangular vocal-tract model with asymmetric wall impedances, in: INTERSPEECH, 2013, pp. 138–142. Lyon, France.
[35] M. Fleischer, S. Pinkert, W. Mattheus, A. Mainka, D. Mürbe, Formant frequencies and bandwidths of the vocal tract transfer function are affected by the mechanical impedance of the vocal tract wall, Biomechanics Model. Mechanobiol. 14 (4) (2015) 719–733.
[36] M. Arnela, R. Blandin, S. Dabbaghchian, O. Guasch, F. Alías, X. Pelorson, A. Van Hirtum, O. Engwall, Influence of lips on the production of vowels based on finite element simulations and experiments, J. Acoust. Soc. Am. 139 (5) (2016) 2852–2859.